

Electronic Supplementary Information

A Fluorescence-Phosphorescence Dual-emissive Cu₃(pyrazolate)₃ Complex with Highly-tunable Emission Colours for Anticounterfeiting and Temperature Sensing

Ze-Miao Xiao, Jing-Xuan Yang, Xu Chen, Wen-Jing Tang, Su-Kao Peng, De-Bo Hao, Ze-Peng Zhao, Ji Zheng,* and Dan Li*

College of Chemistry and Materials Science, Guangdong Provincial Key Laboratory of Functional Supramolecular Coordination Materials and Applications, Jinan University, Guangzhou 510632, China.

E-mail: jizheng@jnu.edu.cn, danli@jnu.edu.cn

Table of Contents

Experimental details.....S3-S6

Synthesis and characterization of **HL1**, **HL2**, **1** and **2**

Fig. S1 ~ S2 (¹H NMR)

Fig. S3 ~ S5 (FT-IR, PXRD and TGA)

Crystal Data.....S7-S8

Table S1 ~ S2 (Structure refinement and crystallographic parameters; Selected geometrical Parameters)

Fig. S6 (The asymmetric units of **1** and **2**)

Photophysical data.....S9-S13

Fig. S7 ~ S8 (Solid-state excitation spectra of **1** and **2**)

Fig. S9 ~ S10 (Solid-state emission spectra of **1** excited under different excitation wavelengths at 77 K and room temperature)

Fig. S11 (Solid-state emission spectra of **1** excited under different excitation wavelengths at different temperatures)

Fig. S12 ~ S14 (Solid-state emission spectra of **2** excited under different excitation wavelengths at different temperatures)

Fig. S15 (Emission decay profiles of **2**)

Table S3 (Summary of luminescent data)

Computational Details.....S14-S22

Table S4 (Selected geometry parameters)

Table S5~S14 (TDDFT results, orbital energy levels and Hirshfeld composition)

Fig. S16~S19 (The contours of selected molecular orbitals)

Reference.....S24

Experimental details

Materials and Measurements

Commercially available reagents and solvents were used without further purification. Fourier Transform infrared spectroscopy was performed using KBr disks on a Thermo Scientific FT-IR Nicolet is 10 spectrometer in the range of 4000~400 cm^{-1} , and abbreviations used for the IR bands are: w = weak, m = medium, b = broad, s = strong, vs = very strong. ^1H NMR spectroscopy was carried out with a Bruker DPX 400 spectrometer using $\text{Si}(\text{CH}_3)_4$ as the internal standard, and all δ values are given in ppm. UV-vis absorption spectra were recorded by a Bio-Logic MOS-500 multifunctional circular dichroism spectrometer. Elemental analyses were carried out with an Elementar vario MICRO CUBE equipment. Powder X-ray diffraction (PXRD) experiments were performed on a Rigaku Ultima IV X-ray diffractometer ($\text{Cu K}\alpha$, $\lambda = 1.5418 \text{ \AA}$) in the step of 0.02° under the conditions 40 KV and 40 mA. Steady-state photoluminescence spectra and emission decay times were recorded by a single-photon counting spectrometer on a Flourolog Horiba spectrofluorometer. Absolute quantum yield was recorded by Hamamatsu C11347-01 absolute PL quantum yield spectrometer under room temperature. Thermogravimetric analysis curve was recorded by TGA Q50 V20.6 with a heating rate of $10 \text{ }^\circ\text{C}/\text{min}$ from 40 to $800 \text{ }^\circ\text{C}$ in a N_2 atmosphere.

Synthesis and characterization

Synthesis of the Ligand 4-anthracen-9-yl-1H-pyrazole(**HL1**)

The synthetic pathway has been demonstrated in Scheme 1a. The detailed process is as follow. A mixture of 1-(2-tetrahydropyranyl)-1H-pyrazole-4-boronic acid pinacol ester (1.20 g, 4.3 mmol), 9-bromoanthracene (0.87 g, 3.4 mmol), K_2CO_3 (4.5 g, 13.8 mmol), and terakis(triphenylphosphine)palladium(0) (1.73 g, 1.5 mmol) was added to a 500 mL round-bottom flask, followed by adding 120 mL of 1,4-dioxane and 30 mL of deionized water. Then the mixture was degassed by three freeze-pump-thaw cycles. After that, the mixture was stirred and heated at $100 \text{ }^\circ\text{C}$ for 48 hours under nitrogen atmosphere, yielding brown liquid, and then extracted with CH_2Cl_2 . The organic phase was concentrated under reduced pressure to afford a yellow oily residue. Finally, the pale-yellow solid was obtained as the intermediate product by purifying the oily residue through column chromatography (petroleum ether/EtOAc = 1/3, v/v). Dissolved the pale-yellow solid in 100 mL of EtOH, followed by adding 30 mL of HCl solution (1 mol/L), and then the resulting solution was stirred and heated at $70 \text{ }^\circ\text{C}$ for 12 hours, in order to remove tetrahydropyranyl group (i.e., the protecting group). After that, the yellow solution was neutralized to $\text{pH} = 7$ by saturated NaHCO_3 aqua solution, and the final products precipitate during the neutralization. Finally, **HL1** was obtained as pale-yellow solid (yield: 53%, based on 9-bromoanthracene). Elemental analyses ($\text{C}_{17}\text{H}_{12}\text{N}_2$, %): calculated: C, 83.58; H, 4.95; N, 11.47; found: C, 84.63; H, 4.74; N, 11.27. FT-IR data (KBr, cm^{-1}): 3120(vs), 2962(vs), 1324(s), 1133(s), 1010(vs), 947(s),

910(s), 885(vs), 844(w), 816(s), 790(vs), 734(vs), 680(m), 625(m), 549(w). ¹H NMR (400 MHz, DMSO-*d*₆, 298 K) δ 13.31 (s, 1H, NH), 8.62 (s, 1H, CH_{An}), 8.12 (d, *J* = 8.3 Hz, 2H, CH_{An}), 8.05 (s, 1H, CH_{Pz}), 7.86 (d, *J* = 8.7 Hz, 2H, CH_{An}), 7.70 (s, 1H, CH_{Pz}), 7.49 (dt, *J* = 15.1, 7.1 Hz, 4H, CH_{An}).

Synthesis of the Ligand 13-phenyl-9-(1H-pyrazol-4-yl)-9,10-dihydro-9,10-[3,4]epipyrrroanthracene-12,14-dione (**HL2**)

The synthetic pathway has been demonstrated in Scheme 1b. The detailed process is as follow. Mixing **HL1** (0.25 g, 1 mmol), N-phenylmaleimide (0.34 g, 2 mmol) in 50 mL of toluene in a 100 mL round-bottom flask, followed by stirring and heating at 100 °C for 12 hours. Finally, the ligand **HL2** was isolated as white powder after filtration (yield: 65%, based on **HL1**). Elemental analyses (C₂₇H₁₉N₃, %): calculated: C, 84.16; H, 4.94; N, 10.91; found: C, 84.09; H, 4.93; N, 10.83. FT-IR data (KBr, cm⁻¹): 3305(s), 1713(vs), 1500(w), 1457(s), 1381(m), 1202(s), 1174(w), 1076(w), 768(m), 752(m), 557(m). ¹H NMR (400 MHz, DMSO-*d*₆) δ 13.08 (s, 1H, NH), 7.91 (s, 2H, CH_{Ph}), 7.56 (d, *J* = 6.8 Hz, 1H, CH_{Ph}), 7.42 - 7.15 (m, 8H, CH_{An}), 7.10 (t, *J* = 7.6 Hz, 1H, CH_{Ph}), 6.57 (d, *J* = 7.5 Hz, 1H, CH_{Ph}), 6.39 (dd, *J* = 6.5, 3.1 Hz, 2H, CH_{Ph}), 4.94 (d, *J* = 3.1 Hz, 1H_{Ph}, CH), 3.93 (d, *J* = 8.3 Hz, 1H, CH), 3.51 (d, *J* = 11.4 Hz, 1H, CH).

Synthesis of **1** (Cu₃(L1)₃)

Into a Pyrex tube with the inside-diameter of 8 mm, **HL1** (5 mg, 0.02 mmol), Cu₂O (2.2 mg, 0.015 mmol), MeCN (1 mL), deionized water (1 mL), and Et₃N (0.1 mL) were added. Then, the tube was flame-sealed and heated to 140 °C in a programmable oven for 72 hours, followed by slow cooling (5 °C/h) to room temperature, yielding the yellow block crystals of **1** (yield: 62%, based on Cu₂O). Elemental analyses (Cu₃C₅₁H₃₃N₆, %): calculated: C, 66.45; H, 3.58; N, 9.12; found: C, 66.36; H, 3.55; N, 9.08. FT-IR data (KBr, cm⁻¹): 1324(m), 1133(s), 1010(vs), 947(s), 910(s), 885(vs), 844(w), 816(s), 790(vs), 734(vs), 680(m), 625(m), 549(w).

Synthesis of **2** (Cu₃(L2)₃)

A Cu(NO₃)₂ solution with the concentration of Cu(II) ions at *ca.* 7.5 × 10⁻³ mol/L was prepared by dissolving Cu(NO₃)₂•3H₂O (36.2 mg, 0.15 mmol) in 20 mL of MeOH. Into a Pyrex tube with the inside-diameter of 8 mm, 2 mL of the above solution containing Cu(II) ions of *ca.* 0.015 mmol was added to mixed with **HL2** (8.3 mg, 0.02 mmol). Then, the tube was flame-sealed and heated to 140 °C in a programmable oven for 72 hours, followed by slow cooling (5 °C/h) to room temperature, yielding the yellow block crystals of **2** (yield: 50%, based on Cu(NO₃)₂•3H₂O). Elemental analyses (Cu₃C₈₁H₅₄N₉O₆, %): calculated: C, 67.50; H, 3.75; N, 8.75; found: C, 67.24; H, 3.64; N, 8.58. FT-IR data (KBr, cm⁻¹): 3467(m), 1713(vs), 1500(w), 1457(w), 1381(m), 1202(w), 1174(w), 1076(w), 768(m), 752(m), 557(m).

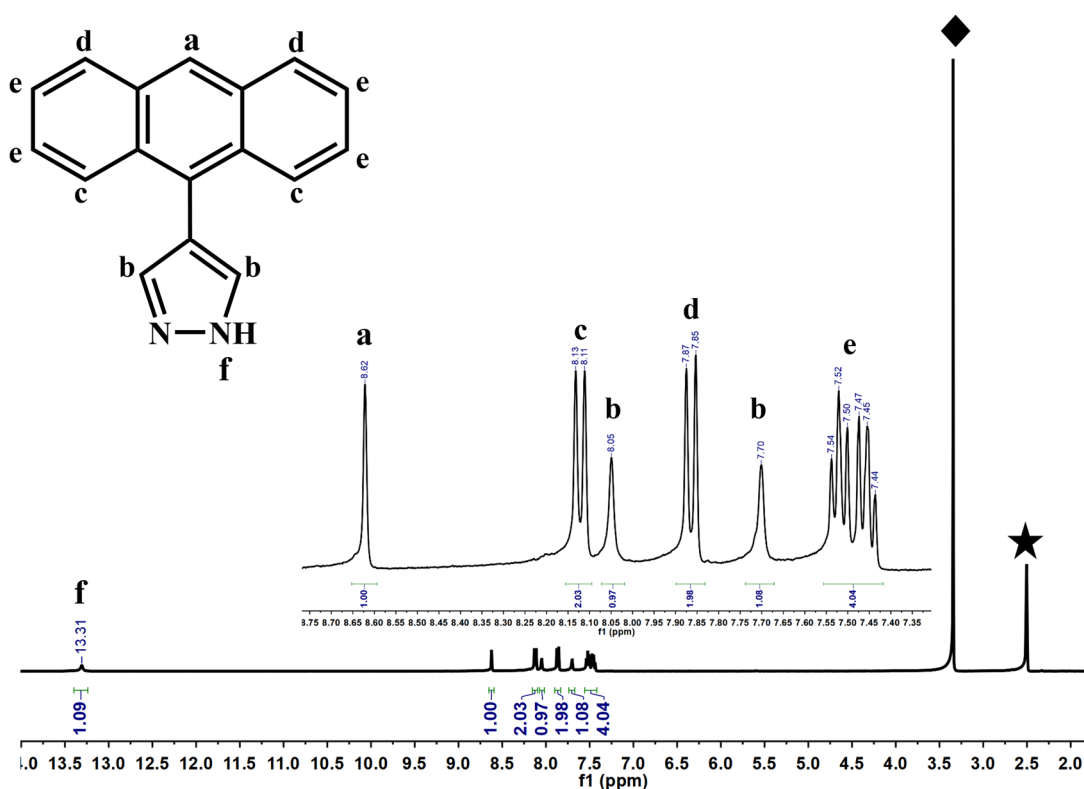


Fig. S1 ^1H NMR (400 MHz, DMSO- d_6 , 298 K) spectrum of **HL1**. Note that pentagram refers to solvent peak and diamond square represents water peak.

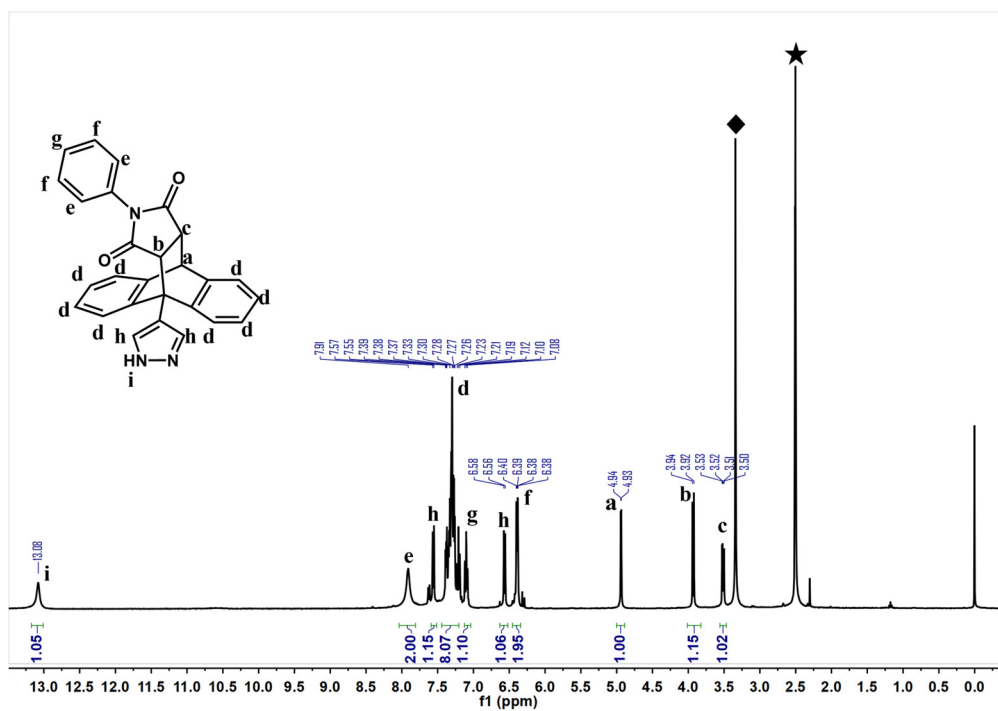


Fig. S2 ^1H NMR (400 MHz, DMSO- d_6 , 298 K) spectrum of **HL2**. Note that pentagram refers to solvent peak and diamond square represents water peak.

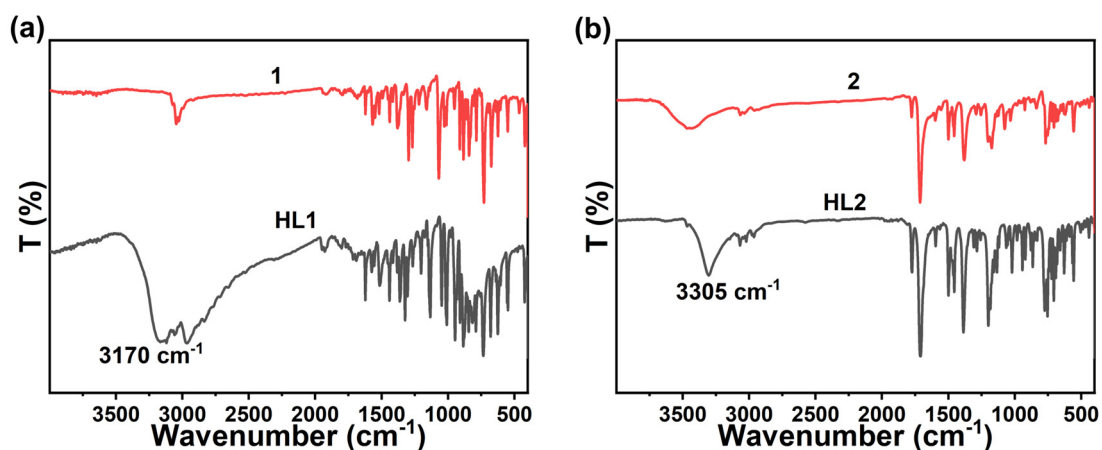


Fig. S3 (a) FT-IR spectra of HL1 and 1,
(b) FT-IR spectra of HL2 and 2.

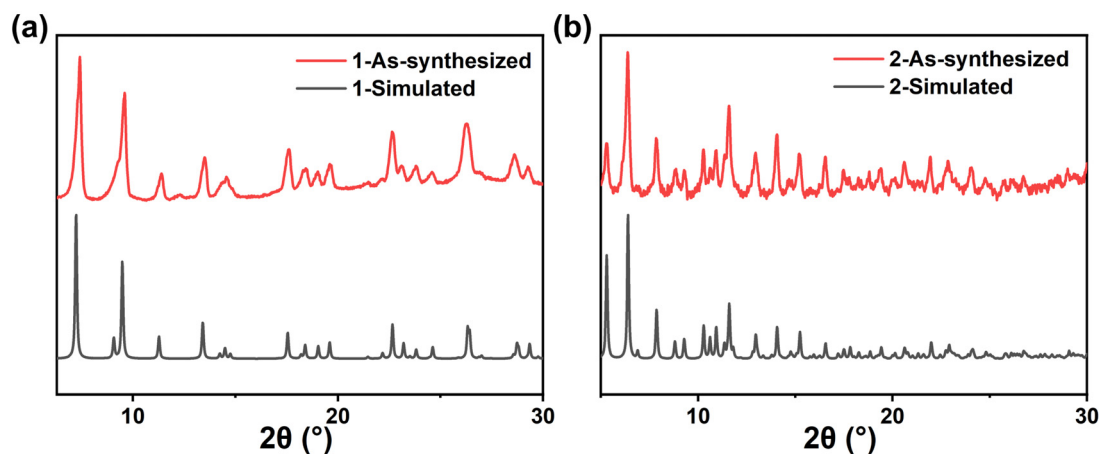


Fig. S4 (a) PXRD patterns of 1, (b) PXRD patterns of 2.

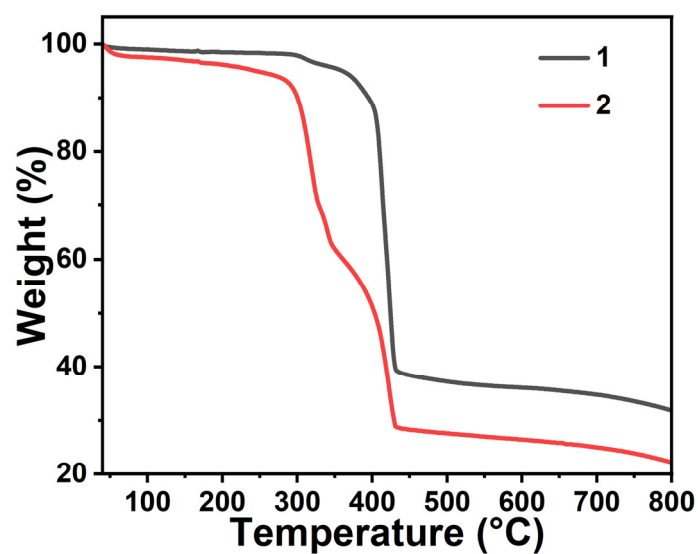


Fig. S5 Thermal gravimetric curves of 1 and 2.

Crystal Data

Suitable single crystals of **1** and **2** were mounted with glue at the end of a glass fiber. Data collection was performed on an Oxford Diffraction XtalAB [Rigaku(Cu) X-ray dual wavelength source, $K\alpha$, $\lambda = 1.5418 \text{ \AA}$] equipped with a monochromator and CCD plate detector (CrysAlisPro CCD, Oxford Diffraction Ltd) at 100 K. Structures were solved by direct methods by ShelXS¹ in Olex2 1.2² and refined on F² using full-matrix least-squares (SHELXL-2016/6¹ in Olex2 1.2²). All non-hydrogen atoms were refined with anisotropic thermal parameters, and all hydrogen atoms were included in calculated positions and refined with isotropic thermal parameters riding on those of the parent atoms. Crystal data and structure refinement parameters are summarized in Table S1. CCDC Nos. 2309536 and 2309156.

Table S1 Crystal data for **1** and **2**.

	1	2
Temperature (K)	100	100
Empirical formula	C ₅₁ H ₃₃ Cu ₃ N ₆	C ₈₁ H ₅₄ Cu ₃ N ₉ O ₆
Formula weight	920.45	1439.95
Crystal system	trigonal	monoclinic
space group	<i>R</i> -3	<i>P</i> 2 ₁ / <i>c</i>
<i>a</i> (Å)	15.6812(3)	16.8386(4)
<i>b</i> (Å)	15.6812(3)	20.0643(7)
<i>c</i> (Å)	27.9464(10)	19.2359(7)
α (°)	90	90
β (°)	90	98.359(3)
γ (°)	120	90
Volume (Å ³)	5951.3(3)	6429.9(4)
<i>Z</i>	6	4
ρ_{calc} (g/cm ³)	1.541	1.487
<i>R</i> _{int}	0.0282	0.0478
Completeness (%)	99.7	99.7
Goodness-of-fit on F ²	1.077	1.034
<i>R</i> ₁ ^a [<i>I</i> > 2σ(<i>I</i>)]	0.0740	0.0951
<i>wR</i> ₂ ^b (all data)	0.2231	0.2899
Largest diff. peak and hole (e/Å ³)	2.24/-0.45	1.11/-0.56

^a $R_1 = \Sigma|F_o| - |F_c|/\Sigma|F_o|$, ^b $wR_2 = \{[\Sigma w(F_o^2 - F_c^2)^2]/\Sigma[w(F_o^2)^2]\}^{1/2}$; $w = 1/[\sigma^2(F_o^2) + (aP)^2 + bP]$, where $P = [\max(F_o^2, 0) + 2F_c^2]/3$ for all data.

Table S2 Selected bond lengths (Å) and angles (°) of **1** and **2**.

1			
Cu(1)-N(1)	1.854(4)	Cu(1)-N(2)#1	1.853(4)
N(1)-Cu(1)-N(2)#1	179.45(19)		
2			
Cu(1)-N(1)	1.836(5)	Cu(1)-N(6)	1.850(5)
Cu(2)-N(2)	1.861(5)	Cu(2)-N(3)	1.847(5)
Cu(3)-N(4)	1.862(5)	Cu(3)-N(5)	1.849(5)
N(1)-Cu(1)-N(6)	172.9(3)	N(2)-Cu(2)-N(3)	175.7(2)
N(5)-Cu(3)-N(4)	175.0(3)		

Symmetry Code: #1 1+Y-X,1-X,+Z.

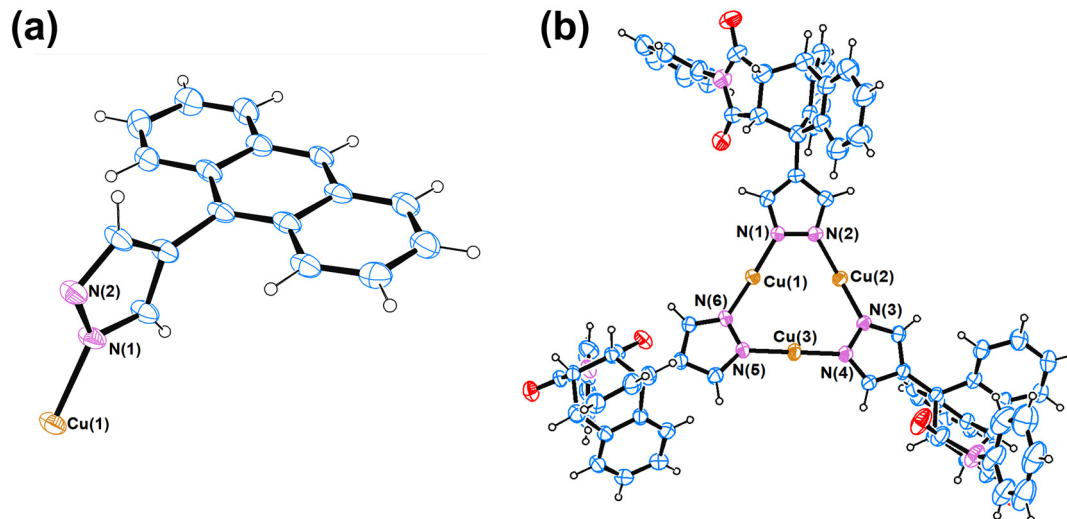


Fig. S6 The asymmetric units of (a) **1** and (b) **2** determined at 100 K shown by ORTEP diagram of 30% probability. Colour code: orange: Cu; pink: N; blue: C; red: O; white: H.

Photophysical Data

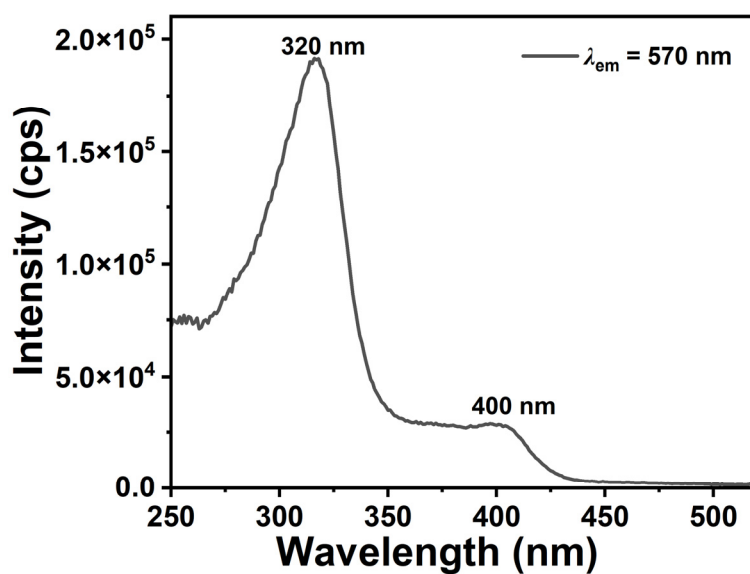


Fig. S7 Solid-state excitation spectra of **1** at room temperature.

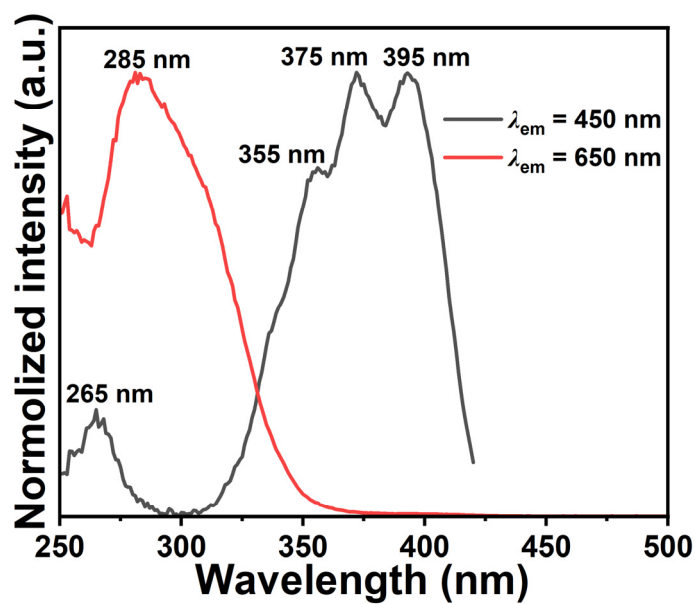


Fig. S8 Solid-state excitation spectra of **2** at room temperature.

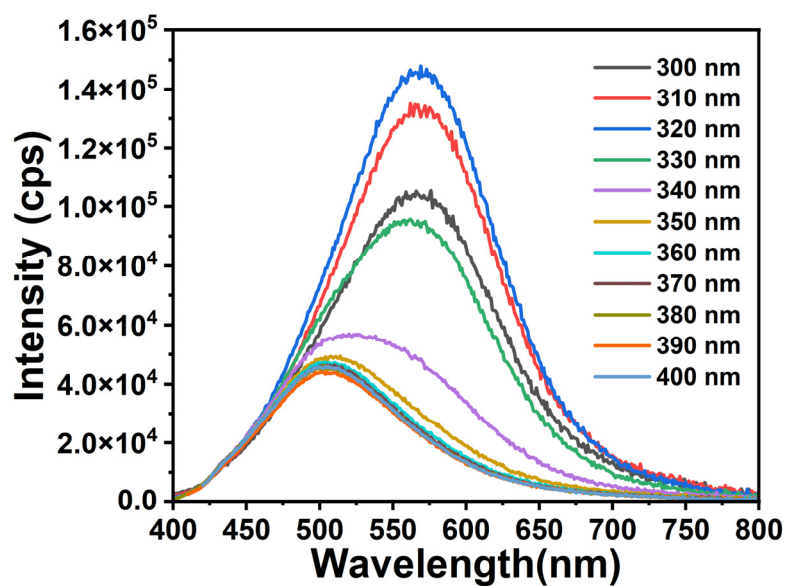


Fig. S9 Solid-state emission spectra of **1** under different excitation wavelengths at room temperature.

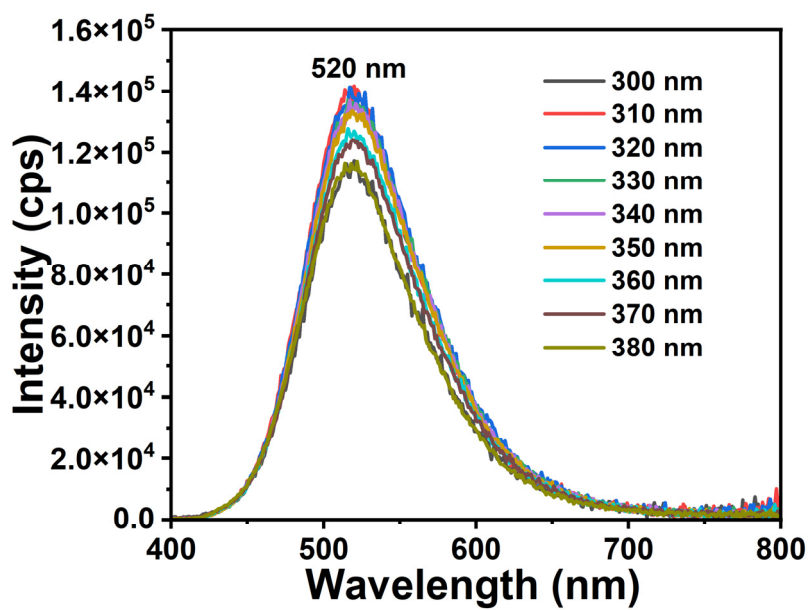


Fig. S10 Solid-state emission spectra of **1** under different excitation wavelengths at 77 K.

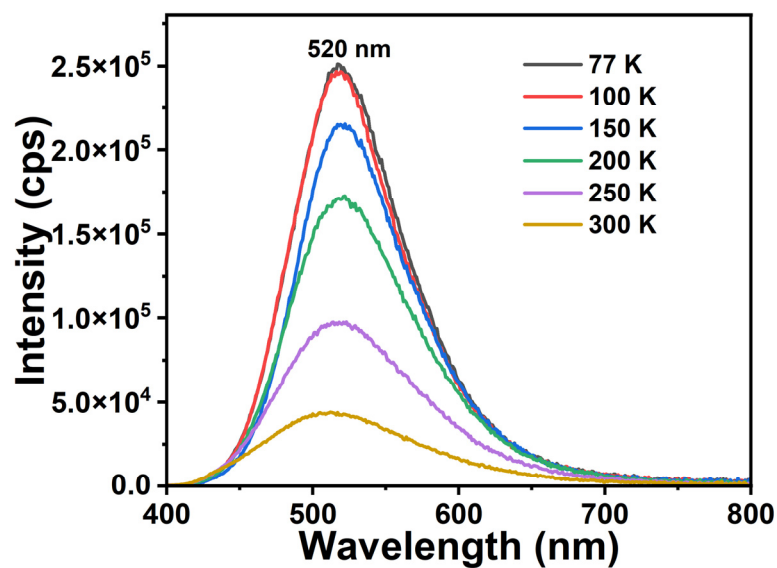


Fig. S11 Solid-state emission spectra of **1** excited at 350 nm at different temperatures.

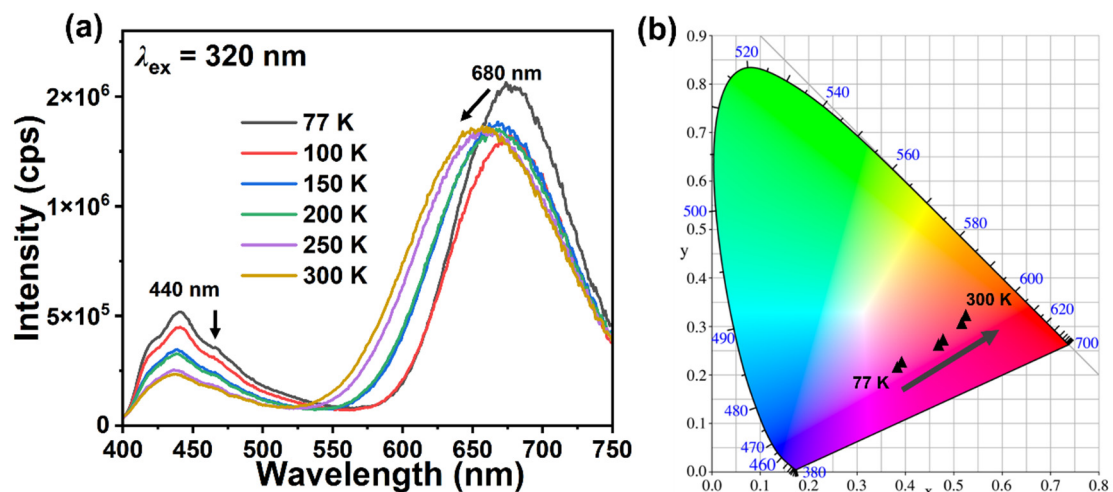


Fig. S12 (a) Solid-state emission spectra of **2** excited at 320 nm at different temperatures. (b) CIE chromaticity diagram of **2** excited at 320 nm at different temperatures.

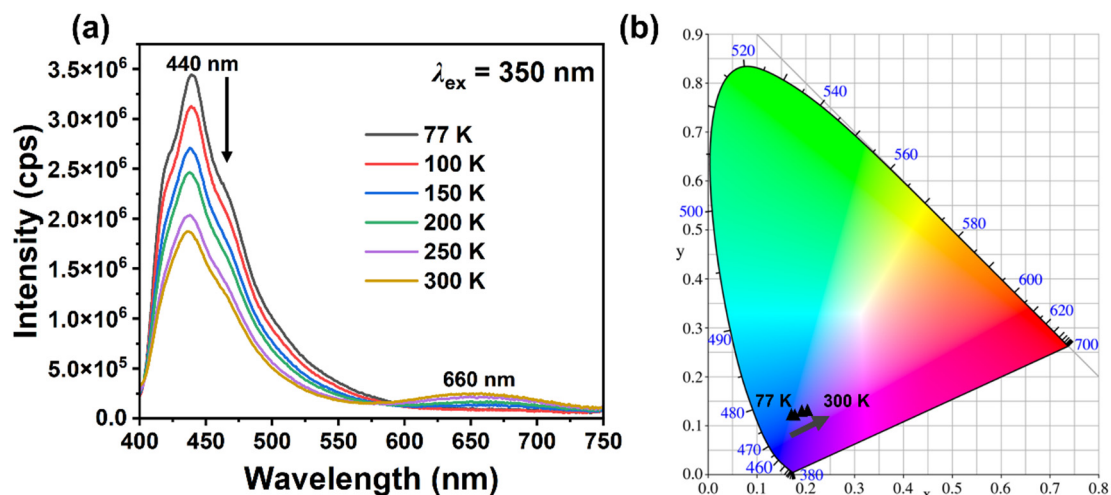


Fig. S13 (a) Solid-state emission spectra of **2** excited at 350 nm at different temperatures. (b) CIE chromaticity diagram of **2** excited at 350 nm at different temperatures.

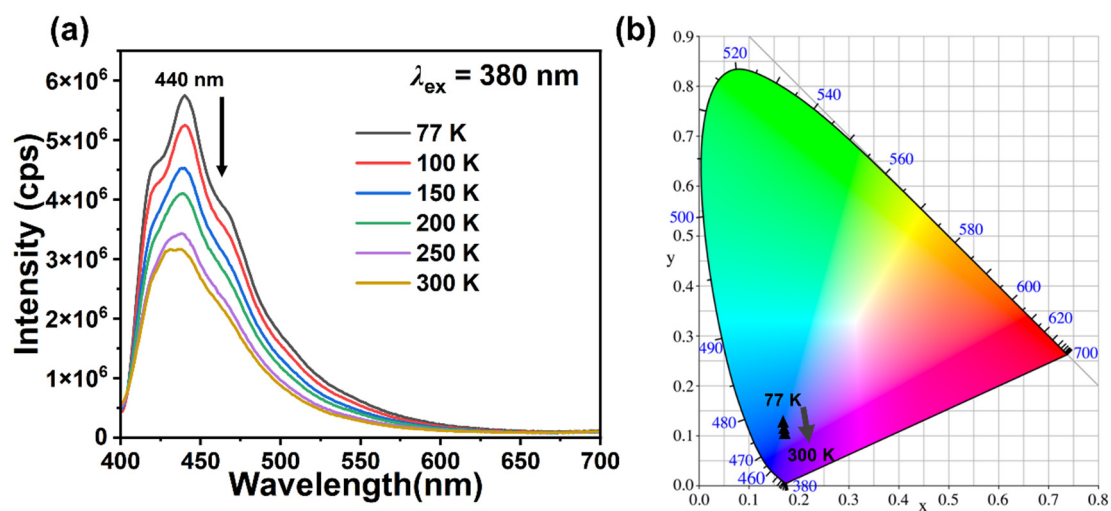


Fig. S14 (a) Solid-state emission spectra of **2** excited at 380 nm at different temperatures. (b) CIE chromaticity diagram of **2** excited at 380 nm at different temperatures.

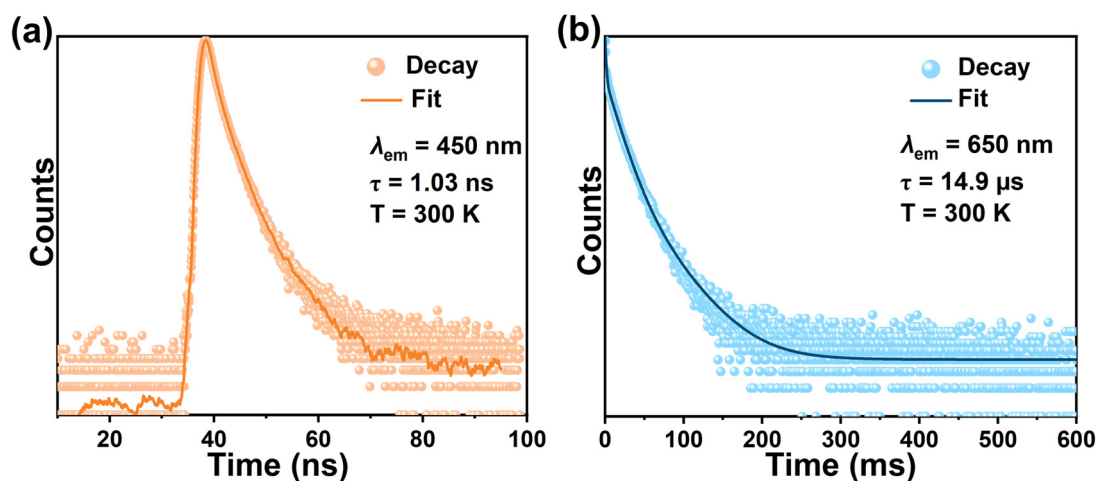


Fig. S15 (a) Emission decay profiles of **2** at room temperature ($\lambda_{\text{ex}} = 370$ nm). (b) Emission decay profiles of **2** at room temperature ($\lambda_{\text{ex}} = 320$ nm).

Table S3 Summary of luminescence data for **HL1**, **HL2**, **1** and **2**.

Compound	State	λ_{abs} (nm)	λ_{ex} (nm)	λ_{em} (nm)	Emission Decay Time	Quantum Yield (%)
HL1	Powder	275, 380, 400	350	490	14.3 ns	-
1 (300 K)	Crystal	290, 380, 400	320	570	0.72 ns	1.5 ($\lambda_{\text{ex}} = 320$ nm)
1 (77 K)	Crystal	-	320	520	-	-
HL2	Powder	325	370	435	0.0065 ns	-
2 (300 K)	Crystal	360, 400	320	650	14.9 μs	4.6 ($\lambda_{\text{ex}} = 370$ nm)
			380	450	1.03 ns	
2 (77 K)	Crystal	-	310	675	879 μs	-
			380	450	1.69 ns	

Computational Details

DFT and TDDFT calculations were conducted by Gaussian 09E³ software. In all calculations, the hybrid functional PBE0-D3(BJ) was adopted in conjunction with SDD⁴ effective core potential (ECP) for copper atoms and 6-311G(d,p)^{5,6} basis set for non-metal atoms. The CTC monomers and dimers of complexes **1** and **2** were selected and optimized to obtain stable geometries at S₀ states, confirmed by frequency calculations. The singlet-singlet spin-allowed transitions and the singlet-triplet spin-forbidden transitions were computed with IOp(9/40=4) based on the optimized models of **1** and **2** as well as the dimer of **2** without optimization. The result files (fchk and log) were furtherly treated by Multiwfn 3.8 software⁷ for extracting the excited-state information, and clarifying the assignments of excited states by (1) generating the cubic files (cub) of electron density difference (EDD) for illustrating EDD maps with isovalue = 0.0005 a.u., (2) illustrating colour-filled TDM maps, and (3) providing Hirshfeld orbital compositions⁸.

Table S4 Comparison of selected bond lengths and bond angles of the structures before and after optimization.

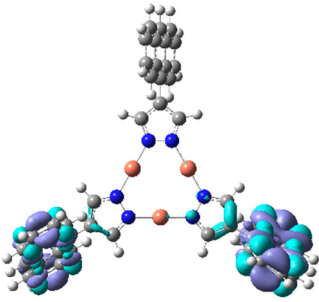
	1			2		
	M(opt) ^a	D(opt) ^b	Crystal (100 K) ^c	M(opt) ^a	D(opt) ^b	Crystal (100 K) ^c
d(Cu-Cu, intra) (Å)	3.226 ~ 3.229	3.206 ~ 3.218	3.204	3.220 ~ 3.242	3.075 ~ 3.319	3.170 ~ 3.267
d(Cu-Cu, inter) (Å)	-	3.372	3.661	-	3.431 ~ 3.447	2.954
d(Cu-N) (Å)	1.853	1.861 ~ 1.868	1.862	1.861 ~ 1.863	1.848 ~ 1.874	1.837 ~ 1.862
N-Cu-N (°)	179.5 ~ 179.6	177.5 ~ 179.0	179.5	178.1 ~ 179.2	173.8 ~ 177.0	172.9 ~ 175.7

^aThe optimized monomer in ground state.

^bThe optimized dimer in ground state.

^cThe crystal structure at 100 K.

Table S5 Selected TDDFT results of the optimized monomer of **1** (**1M**).

Excited State	E (eV)	λ (nm)	f	EDD map
S ₁	3.217	385.4	0.2306	

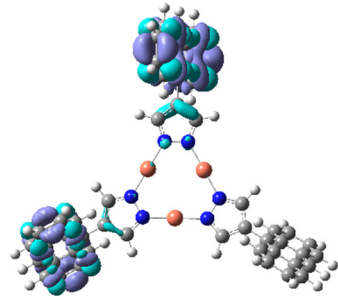
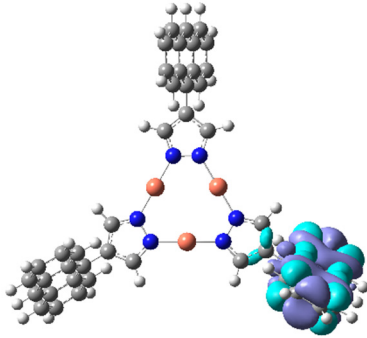
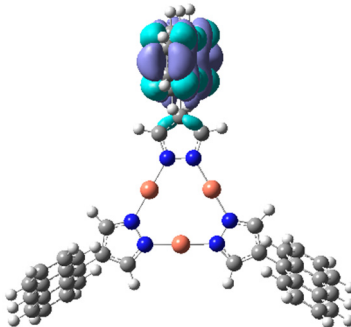
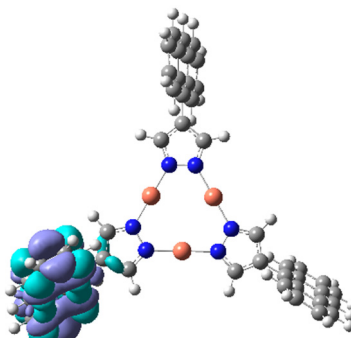
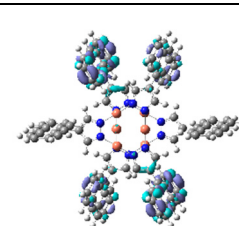
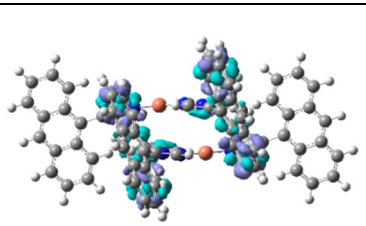
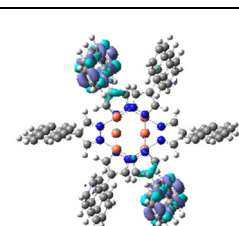
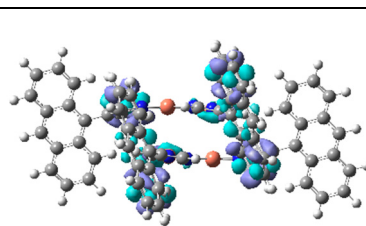
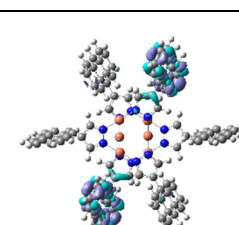
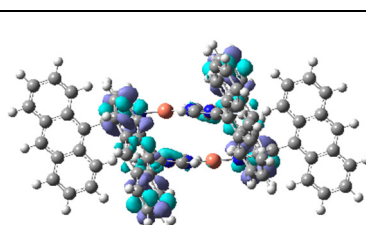
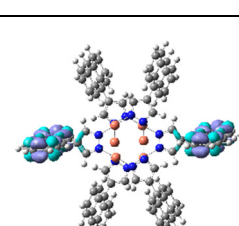
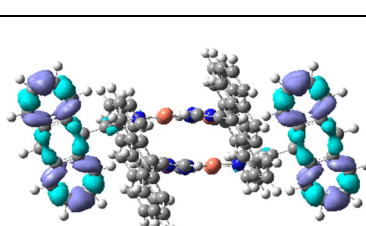
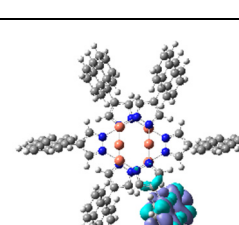
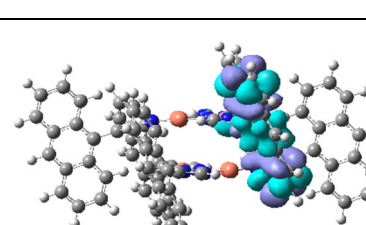
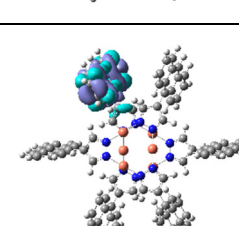
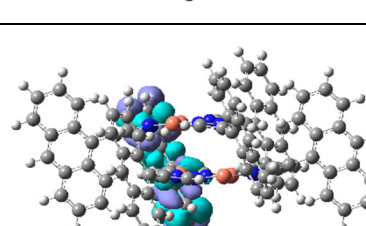
S ₂	3.217	385.4	0.2296	
T ₁	1.658	748.0	0.0000	
T ₂	1.658	747.9	0.0000	
T ₃	1.658	747.8	0.0000	

Table S6 The orbital energy level (OEL, in eV) and the Hirshfeld composition (%) of each selected molecular orbital in **1M**.

	H-3	H-2	H-1	H	L	L+1	L+2	L+3
OEL	-6.733	-5.610	-5.600	-5.599	-1.808	-1.806	-1.804	-0.581
Cu	41.28	0.62	0.59	0.97	0.17	0.12	0.08	75.18
Pz	50.46	5.56	6.49	6.69	3.40	3.58	3.50	23.17
An	8.11	93.99	93.00	92.60	96.54	96.58	96.62	1.47

Table S7 Selected TDDFT results of the optimized dimer of **1 (1D)**.

Excited State	E (eV)	λ (nm)	f	EDD map	
				Top View	Side View
S ₁	3.152	393.4	0.000		
S ₂	3.156	392.9	0.143		
S ₃	3.176	390.4	0.469		
S ₅	3.226	384.3	0.330		
T ₁	1.646	753.1	0.000		
T ₂	1.646	753.1	0.000		

T ₃	1.651	751.1	0.000		
T ₆	1.664	745.1	0.000		

Table S8 The orbital energy level (OEL, in eV) and the Hirshfeld composition (%) of each selected molecular orbital in **1D**.

	H-6	H-5	H-4	H-3	H-2	H-1	H
OEL	-6.394	-5.601	-5.596	-5.583	-5.577	-5.567	-5.558
Cu	72.51	0.62	0.95	0.95	1.46	0.96	1.32
Pz	23.68	5.83	6.09	8.13	7.82	8.60	10.30
An	3.80	93.55	92.95	90.92	90.72	90.45	88.38
	L	L+1	L+2	L+3	L+4	L+5	L+6
OEL	-1.826	-1.824	-1.819	-1.817	-1.783	-1.782	-0.968
Cu	0.72	0.30	0.21	0.19	0.15	0.12	64.57
Pz	4.20	3.91	3.97	4.12	3.23	3.25	29.48
An	95.08	95.79	95.83	95.69	96.62	96.63	5.95

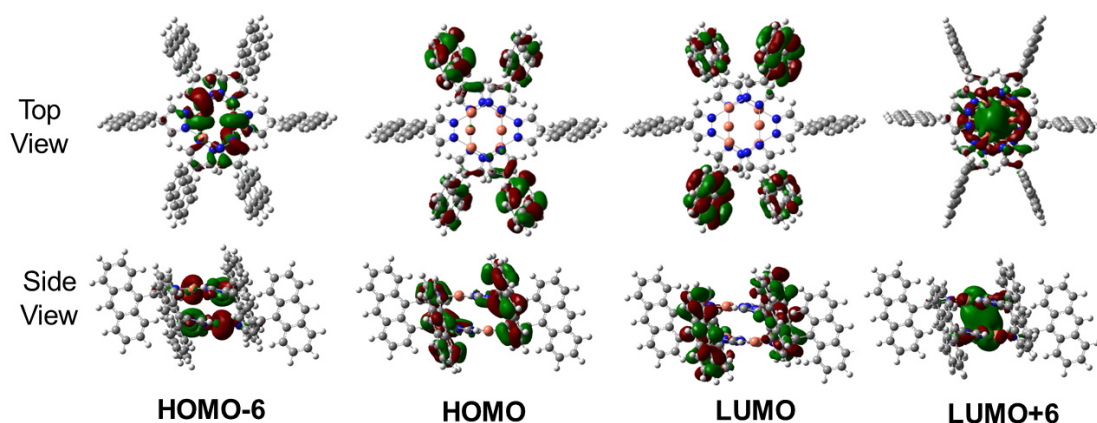
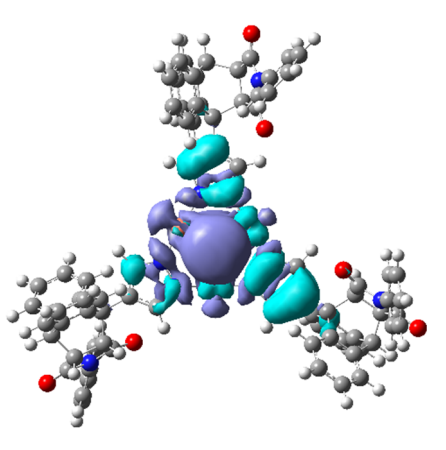
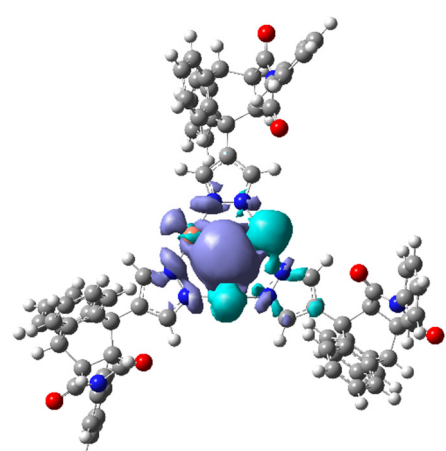
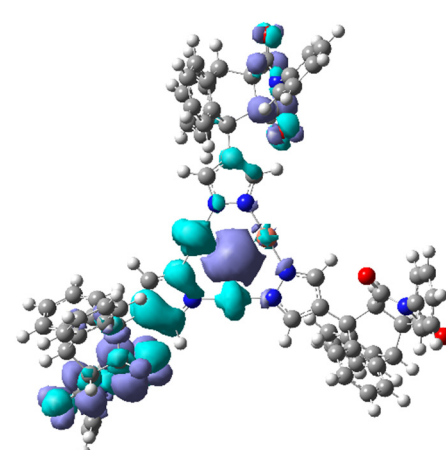


Fig. S16 The contours of selected molecular orbitals of **1D**. (isovalue = 0.02).

Table S9 Selected TDDFT results of the singlet-singlet spin-allowed transitions ($S_0 \rightarrow S_n$) of the optimized monomer of **2** (**2M**).

S_n	E (eV)	λ (nm)	f	EDD map
-------	--------	----------------	-----	---------

S ₁	4.757	260.6	0.000	
S ₃	4.857	255.3	0.050	
S ₄	4.886	253.7	0.014	

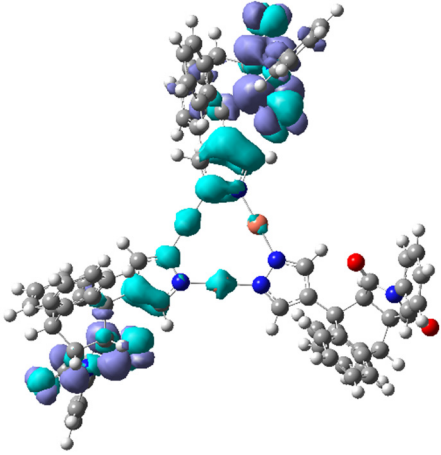
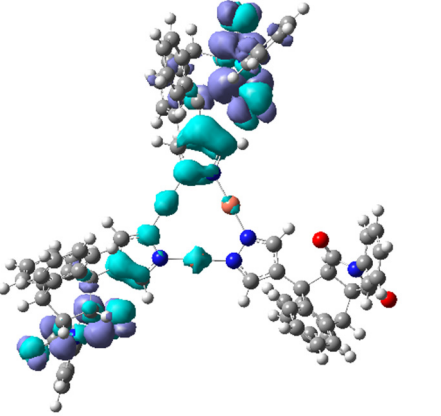
S ₅	4.893	253.4	0.038	
S ₆	4.906	252.7	0.060	

Table S10 The orbital energy level (OEL, in eV) and the Hirshfeld composition (%) of each selected molecular orbital in **2M**.

	H	L	L+1	L+2	L+3	L+4
OEL	-6.508	-0.713	-0.697	-0.628	-0.557	-0.551
Cu	24.92	0.16	0.16	0.19	1.78	1.18
Pz	61.13	1.21	1.16	1.02	1.85	2.57
DA	13.95	98.63	98.68	98.79	96.37	96.24
	L+5	L+6	L+7	L+8	L+9	L+10
OEL	-0.537	-0.531	-0.518	-0.464	-0.455	-0.441
Cu	0.44	0.48	1.04	11.24	6.15	25.12
Pz	0.63	2.20	2.75	4.25	2.99	8.41
DA	98.94	97.32	96.21	84.52	90.86	66.46

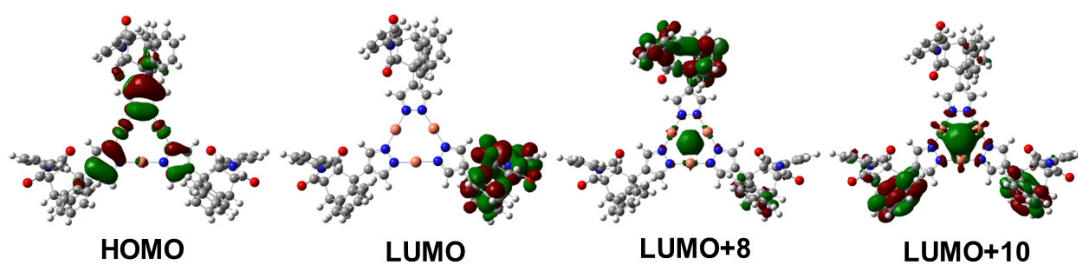


Fig. S17 The contours of selected molecular orbitals of **2M**. (isovalue = 0.02).

Table S11 Selected TDDFT results of **2D**.

Excited State	E (eV)	λ (nm)	f	EDD map	
				Top View	Side View
S ₁	4.349	285.1	0.000		
S ₃	4.484	276.5	0.035		
S ₅	4.551	272.4	0.101		
T ₁	3.537	350.5	0.000		
T ₂	3.537	350.5	0.000		

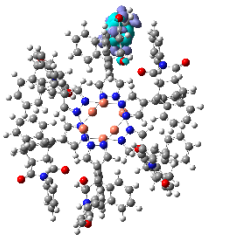
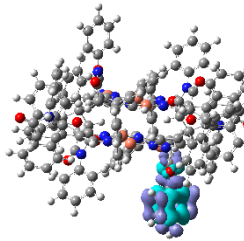
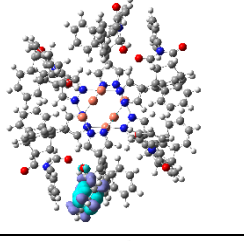
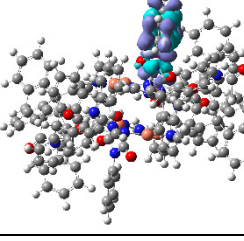
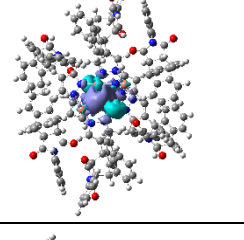
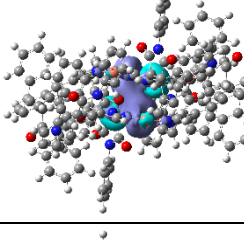
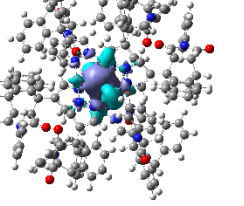
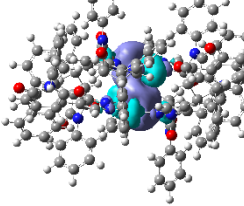
T ₃	3.544	349.9	0.000		
T ₄	3.544	349.9	0.000		
T ₅	3.544	349.9	0.000		
T ₆	3.550	349.3	0.000		

Table S12 The orbital energy level (OEL, in eV) and the Hirshfeld composition (%) of each selected molecular orbital of **2D**.

	H	L	L+1	L+2	L+3	L+4	L+5	L+6
OEL	-6.033	-0.858	-0.839	-0.809	-0.799	-0.780	-0.774	-0.685
Cu	77.62	5.16	0.87	0.68	0.15	0.19	0.21	0.17
Pz	19.46	6.25	3.26	1.55	1.51	1.16	1.24	1.83
DA	2.90	88.56	95.88	97.77	98.33	98.65	98.56	98.01
	L+7	L+8	L+9	L+10	L+11	L+12	L+13	L+14
OEL	-0.684	-0.641	-0.636	-0.608	-0.607	-0.590	-0.581	-0.557
Cu	0.57	1.55	0.18	0.37	0.21	6.66	0.35	13.22
Pz	2.27	2.37	1.50	0.96	0.84	6.07	2.00	8.06
DA	97.17	96.08	98.32	98.67	98.96	87.28	97.65	78.73

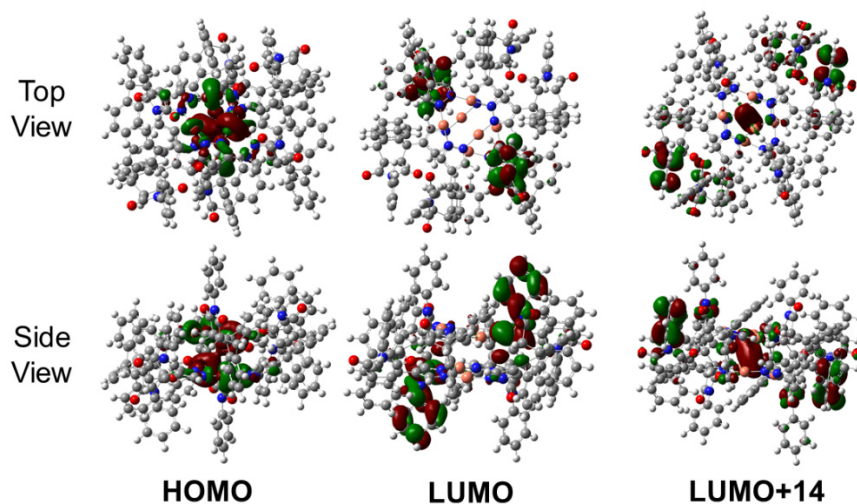


Fig. S18 The contours of selected molecular orbitals of **2D**. (isovalue = 0.02).

Table S13 The orbital energy level (OEL, in eV) and the Hirshfeld composition (%) of each selected molecular orbital of **2D(SC)**.

	H	L	L+1	L+2	L+3	L+4
OEL	-5.832	-0.988	-0.987	-0.794	-0.793	-0.720
Cu	76.88	0.18	0.20	0.43	0.37	0.13
Pz	21.83	1.60	1.53	1.31	1.25	0.68
DA	1.28	98.22	98.27	98.26	98.38	99.19
	L+5	L+6	L+7	L+8	L+9	L+10
OEL	-0.719	-0.717	-0.716	-0.602	-0.601	-0.579
Cu	0.08	0.30	0.21	0.38	0.12	38.35
Pz	0.46	1.04	1.03	0.71	0.59	21.40
DA	99.46	98.68	98.76	98.91	99.28	40.24

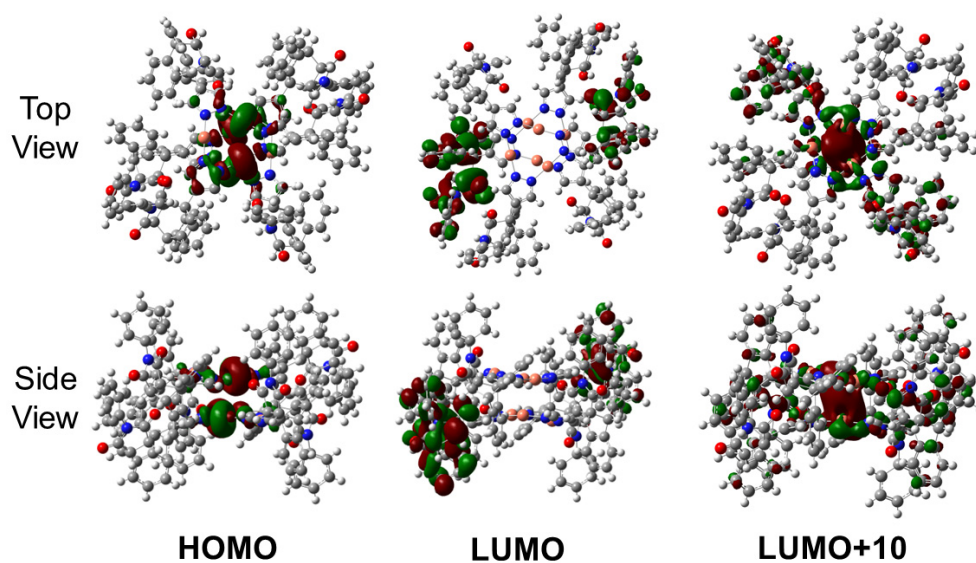


Fig. S19 The contours of selected molecular orbitals of **2D(SC)** (isovalue = 0.02).

Table S14 The orbital energy levels of the calculate models in this work (H = HOMO, L = LUMO).

	1M	1D	2M	2D	2D(SC)
L(Cu-Cu) ^a (eV)	-0.581	-0.968	-0.441	-0.557	-0.579
H(Cu) ^b (eV)	-6.733	-6.394	-6.508	-6.033	-5.832
Gap ^c (eV)	6.152	5.426	6.067	5.476	5.253

^aThe lowest unoccupied molecular orbital displaying the significant Cu-Cu bonding character.

^bThe highest occupied molecular orbital displaying significant contributions from the d orbitals of Cu.

^cThe gap between L(Cu-Cu) and H(Cu).

Reference

- S1 G. M. Sheldrick, A short history of SHELX. *Acta Cryst.*, 2007, **64**, 112-122.
- S2 O. V. Dolomanov, L. J. Bourhis, R. J. Gildea, J. A. K. Howard and H. Puschmann, OLEX2: a complete structure solution, refinement and analysis program. *J. Appl. Crystallogr.*, 2009, **42**, 339-341.
- S3 G. W. T. M. J. Frisch, H. B. Schlegel, G. E. Scuseria, M. A. Robb, J. R. Cheeseman, G. Scalmani, V. Barone, G. A. Petersson, H. Nakatsuji, X. Li, M. Caricato, A. V. Marenich, J. Bloino, B. G. Janesko, R. Gomperts, B. Mennucci, H. P. Hratchian, J. V. Ortiz, A. F. Izmaylov, J. L. Sonnenberg, Williams, F. Ding, F. Lipparini, F. Egidi, J. Goings, B. Peng, A. Petrone, T. Henderson, D. Ranasinghe, V. G. Zakrzewski, J. Gao, N. Rega, G. Zheng, W. Liang, M. Hada, M. Ehara, K. Toyota, R. Fukuda, J. Hasegawa, M. Ishida, T. Nakajima, Y. Honda, O. Kitao, H. Nakai, T. Vreven, K. Throssell, J. A. Montgomery Jr., J. E. Peralta, F. Ogliaro, M. J. Bearpark, J. J. Heyd, E. N. Brothers, K. N. Kudin, V. N. Staroverov, T. A. Keith, R. Kobayashi, J. Normand, K. Raghavachari, A. P. Rendell, J. C. Burant, S. S. Iyengar, J. Tomasi, M. Cossi, J. M. Millam, M. Klene, C. Adamo, R. Cammi, J. W. Ochterski, R. L. Martin, K. Morokuma, O. Farkas, J. B. Foresman and D. J. Fox, Fox, Gaussian 09, Revision E.01. 2009.
- S4 W. Küchle, M. Dolg, H. Stoll and H. Preuss, Energy-adjusted pseudopotentials for the actinides. Parameter sets and test calculations for thorium and thorium monoxide. *J. Chem. Phys.*, 1994, **100**, 7535-7542.
- S5 R. Krishnan, J. S. Binkley, R. Seeger and J. A. Pople, Self-consistent molecular orbital methods. XX. A basis set for correlated wave functions. *J. Chem. Phys.*, 2008, **72**, 650-654.
- S6 A. D. McLean and G. S. Chandler, Contracted Gaussian basis sets for molecular calculations. I. Second row atoms, $Z=11-18$. *J. Chem. Phys.*, 2008, **72**, 5639-5648.
- S7 T. Lu and F. Chen, Multiwfn: A multifunctional wavefunction analyzer. *J. Comput. Chem.*, 2012, **33**, 580-592.
- S8 F. L. Hirshfeld, Bonded-atom fragments for describing molecular charge densities. *Theor. Chim. Acta.*, 1977, **44**, 129-138.